

Development of ultralow energy (1–10 eV) ion scattering spectrometry coupled with reflection absorption infrared spectroscopy and temperature programmed desorption for the investigation of molecular solids

Soumabha Bag,¹ Radha Gobinda Bhui,¹ Rabin Rajan J. Methikkalam,¹ T. Pradeep,^{1,a)} Luke Kephart,² Jeff Walker,² Kevin Kuchta,² Dave Martin,² and Jian Wei²

¹*DST Unit of Nanoscience (DST UNS), Department of Chemistry, Indian Institute of Technology Madras, Chennai 600036, India*

²*Extrel CMS, LLC, 575 Epsilon Drive, Pittsburgh, Pennsylvania 15238, USA*

(Received 26 September 2013; accepted 2 December 2013; published online 17 January 2014)

Extremely surface specific information, limited to the first atomic layer of molecular surfaces, is essential to understand the chemistry and physics in upper atmospheric and interstellar environments. Ultra low energy ion scattering in the 1–10 eV window with mass selected ions can reveal extremely surface specific information which when coupled with reflection absorption infrared (RAIR) and temperature programmed desorption (TPD) spectroscopies, diverse chemical and physical properties of molecular species at surfaces could be derived. These experiments have to be performed at cryogenic temperatures and at ultra high vacuum conditions without the possibility of collisions of neutrals and background deposition in view of the poor ion intensities and consequent need for longer exposure times. Here we combine a highly optimized low energy ion optical system designed for such studies coupled with RAIR and TPD and its initial characterization. Despite the ultralow collision energies and long ion path lengths employed, the ion intensities at 1 eV have been significant to collect a scattered ion spectrum of 1000 counts/s for mass selected CH_2^+ . © 2014 AIP Publishing LLC. [<http://dx.doi.org/10.1063/1.4848895>]

I. INTRODUCTION

Low energy ion scattering (LEIS), where mass selected ions in the 10–100 eV energy range collide on a well-defined surface and the product ions are mass analyzed, is an extremely surface sensitive,¹ molecule specific,² and structure specific³ tool attracting significant attention these days.^{4–6} Chemical reactivity of polyatomic ions at low energies and the capability to confine them in a spatially specific fashion with energy^{7–10} and angle resolution^{11,12} have made it possible to explore novel phenomena using this technique. Precise control of ions has made it possible to soft-land ions at surfaces,⁵ which has implications to chemistry, biology, and devices. As the interaction time scale is of the order of a few femtoseconds,¹³ a surface being sampled may be considered as frozen in the time scale of ion collision.¹⁴ This allows temperature dependent dynamics^{15,16} to be probed efficiently. The capacity to modify surfaces at atomic resolution provides new capability to study model systems.

The ultralow energy analog of LEIS is a new variant wherein translational energy of the incoming ion is as low as 1 eV,^{17,18} such ions are structure sensitive¹⁹ besides their extreme surface specificity, allowing phenomena such as phase transitions to be studied precisely.^{17,20} Coupled with novel surfaces, prepared by a combination of methods such as background deposition, thermal evaporation, sputtering, photochemistry, etc. can create completely new avenues hitherto unexplored.

These studies using LEIS are complementary to diverse analytical methods,^{5,21–33} which are normally used to understand molecular surfaces. All of these experimental capabilities must be built around cryogenic conditions^{28,34} as well as in environments which can maintain ultralow energy ions. While efforts to create, mass select and transfer ultralow energy ions to well-defined molecular surfaces face challenges in effective ion transmission, there are also hardware restrictions to implement spectroscopies around single crystal surfaces for simultaneous experimentation.

The surface chemistry of various molecular solids at different temperature and low pressures is interesting^{34–36} which motivated us to design advanced instrumentation for detailed investigations. In the following, we describe ultralow energy ion scattering spectrometry coupled with reflection absorption infrared spectroscopy (RAIRS) and temperature programmed desorption (TPD), performed in the 10–1000 K window. The experimental capabilities in terms of diversity of measurements and wealth of data are described which present new possibilities to explore fundamental problems of molecular solids.

II. EXPERIMENTAL

Figure 1 shows an outline of the instrument. A detailed description of mass spectrometer components is given in Fig. 2(b) and will be discussed later. The entire vacuum system is composed of three main chambers [ionization (items 2 and 3), octupole (item 6), and scattering] and a sample manipulator on which a closed cycle He-cryostat is mounted. The interior surface of the chamber was polished by buffing to re-

^{a)} Author to whom correspondence should be addressed. Electronic mail: pradeep@iitm.ac.in

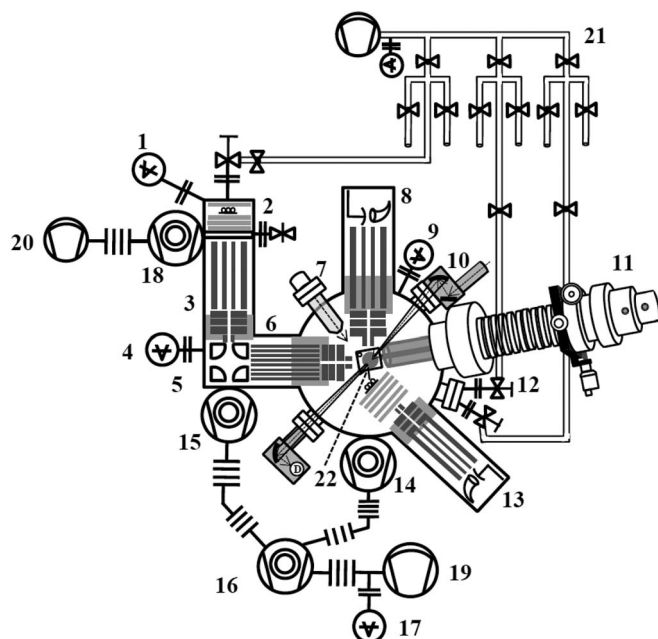


FIG. 1. Schematic of the instrument. Various parts of the instrument are: 1. ionization chamber B-A gauge, 2. ionization chamber, 3. quadrupole mass filter (Q1), 4. octupole chamber cold cathode gauge, 5. ion bender, 6. octupole chamber, 7. low energy alkali ion gun (Cs^+/Li^+), 8. quadrupole mass analyzer (Q3), 9. scattering chamber B-A gauge, 10. RAIRS setup with KBr view port and external MCT detector (D), 11. sample manipulator fitted with closed cycle He-cryostat, 12. scattering chamber leak valves, 13. TPD probe fitted with ionizer and quadrupole mass analyzer and detector, 14. scattering chamber turbomolecular pump (685 l/s), 15. octupole chamber turbo molecular pump (260 l/s), 16. Backing turbo molecular pump (260 l/s), 17. Pirani gauge, 18. ionization chamber turbomolecular pump (80 l/s), 19. diaphragm pump (9.6 m^3/h), 20. diaphragm pump (3.8 m^3/h), 21. gas manifold arrangement with shutoff valve, gas line, pirani gauge, and diaphragm pump, and 22. Ru(0001) single crystal. Standard vacuum symbols are used (wherever necessary) for clarity.

duce outgassing. The ionization chamber is fitted with a 67 l/s turbomolecular pump (TMP, HiPace 80, Pfeiffer Vacuum) marked as item 18. This TMP is backed by a Pfeiffer Vacuum dry pump (MVP 70-3, pumping capacity 3.8 m^3/h) (item 20). In the octupole chamber, the vacuum was created by one HiPace 300 TMP (capacity 260 l/s, Pfeiffer Vacuum) (item 15). The scattering chamber is evacuated by HiPace 700 TMP (capacity 685 l/s, Pfeiffer Vacuum) (item 14). The octupole chamber and the scattering chamber TMPs are backed by another HiPace 300 (Pfeiffer Vacuum) TMP (item 16) which is further backed by a diaphragm pump (MVP 160-3 from Pfeiffer vacuum, pumping capacity 9.6 m^3/h) (item 19). All the TMPs are connected to the vacuum chambers through vibration dampers of appropriate dimensions to overcome any vibrational interference arising from the TMPs. The pressure readings in ionization and scattering chambers are measured using Bayard-Alpert type (B-A gauge, model no. PBR 260) (items 1 and 9, respectively) ionization gauges and the octupole chamber pressure is measured by a cold cathode gauge (IKR 270) with a limit of 5×10^{-11} mbar (item 4), all these sensors are controlled by a “MaxiGauge” vacuum gauge controller (Pfeiffer, Model TPG 256 A). An ultimate pressure below 5×10^{-10} mbar (limit of the sensor) was achieved in both ionization and scattering chambers after bake-out. The octupole chamber pressure is recorded to be 1×10^{-10} mbar.

During the experiment, the sample vapor, i.e., water or other vapors and gases are introduced into the scattering chamber through leak valve (Pfeiffer Vacuum) (item 12). The sample lines of the gas manifold (item 21) are pumped by a small diaphragm pump (MVP 015-4 from Pfeiffer Vacuum), and the samples are separated from the sample line by shut off valves (from Swagelok). The ionization chamber and octupole chamber are separated by a differential pumping baffle and a gate valve, the ions are transferred from the ionization region to the scattering region via the quadrupole mass filter (Q1) (item 3), followed by an ion bender (or ion deflector, item 5). Ions are guided from the octupole chamber to the scattering chamber, through an octupole ion guide. The alignment of ion optical components is achieved using standard laser transit procedures. Argon gas was introduced into the ionization chamber through a leak valve during the experiment when the pressure in it was raised to 2×10^{-7} mbar. The pressure measured in the scattering chamber during experimental condition, i.e., when the Ar source was open, was 1×10^{-9} mbar, which is an indication of effective differential pumping. This was achieved by a gate valve between Q1 and ionization chamber which also incorporates a tube lens. There was an additional vacuum restriction between ionization chamber and the Q1 which further reduces gas flow from the ion source to Q1. The pressure was monitored using a Maxi-Gauge multichannel monitoring system as mentioned before.

A high precision UHV specimen translator (McAllister Corporation) with xyz axis movement and θ rotation facility (item 11) was used as the substrate holder. The substrate holder is made of oxygen free high conductivity (OFHC) copper, and the rest of the spectrometer is made with non-magnetic stainless steel. The mounting copper is electrically isolated from the supporting structure. The heating element is also made of copper. A 1.5 cm diameter ruthenium (Ru) single crystal, Ru(0001) single crystal with 1 mm thickness (point 22) was used as the substrate for deposition during the experiment. This single crystal was mounted on a copper holder which was connected with a closed cycle helium cryostat (from ColdEdge Technologies) through an interface. A heater was also connected to the interface which was electrically isolated from the rest of holder by sapphire balls. Three temperature sensors were connected around the substrate to measure accurately the temperature in the whole range of 10–1000 K. A silicon diode sensor was connected to the top of the interface which measured the cold end of the interface, a Pt-sensor and a K-type thermocouple were attached to the mounting copper (Cu) near to Ru(0001), which was used as the substrate for the growth of molecular solids. The Ru substrate was fixed on the Cu plate by a thin steel clip. The temperature gradient across the sample plate was close to zero. Sample cooling was achieved by a closed cycle He-cryostat and the minimum temperature attained was 7 K whereas the maximum temperature recorded was 1000 K. The sample plate was mounted on the rod connected to the He cryostat. The rod was covered with a polished stainless steel radiation shield. Temperature up to 10 K can be achieved within 2 h, and the variable heating rates like 0.1–50 K/min was controlled by a LakeShore temperature controller (Model 336).

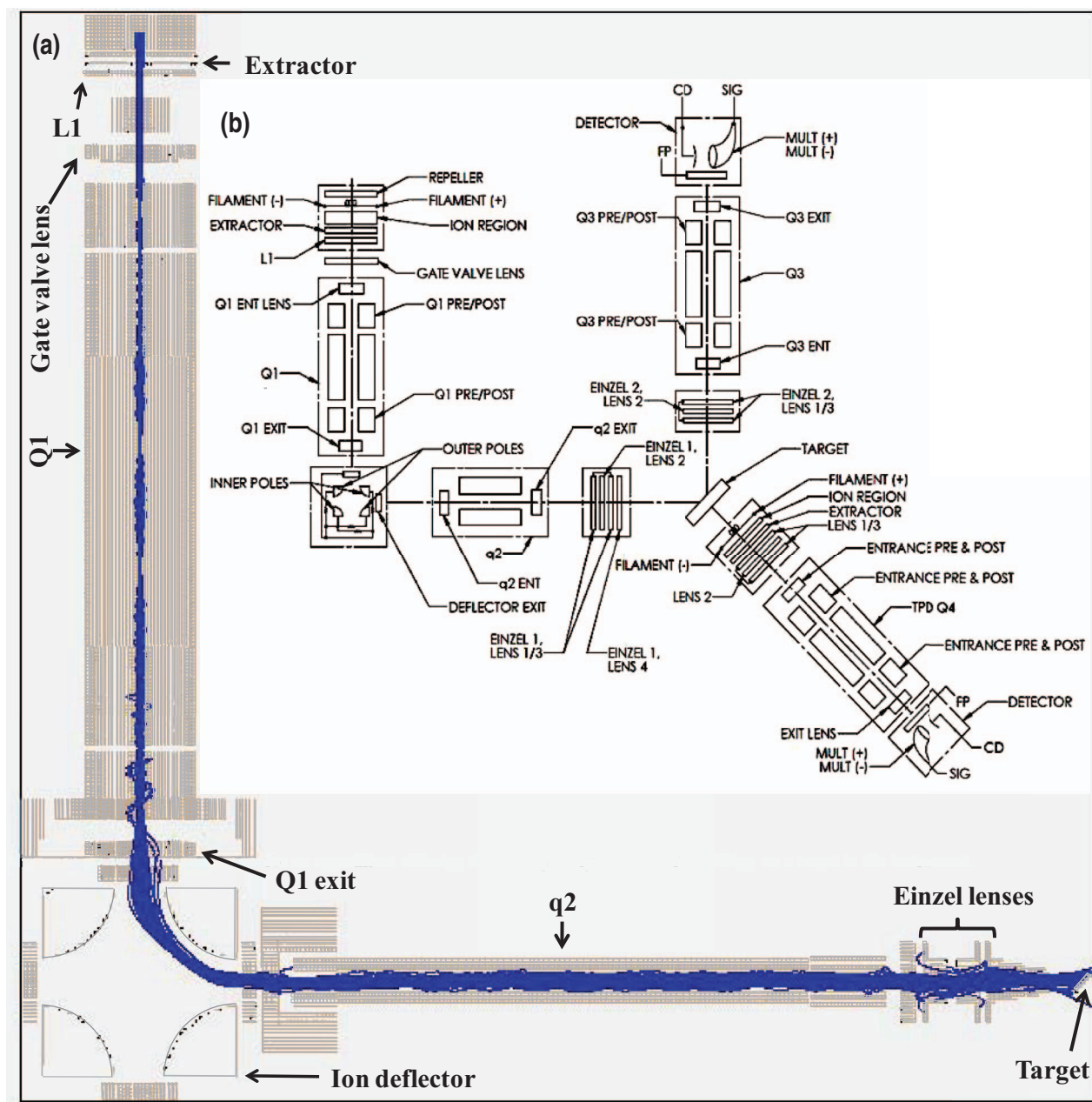


FIG. 2. (a) SimIon simulation of the ion trajectory of 1 eV Ar^+ (m/z 40), colliding on the target. (b) A schematic of the instrument with a description of the components. Appropriate labels are shown on the calculated trajectory so as to relate (a) and (b).

Electron impact ionization (EI) source from Extrel Core Mass Spectrometers (Extrel CMS) was used to generate positive or negative ions. The ionization chamber was fitted with a chamber heater inside the chamber to get the cleaner environment. The generated ions were extracted from the source and transferred to a quadrupole mass filter (Q1) through a set of einzel lenses. The desired mass-to-charge ratio was allowed to pass through Q1. It is possible to get the projectile ions with varying collision energy from 1 to 100 eV by varying the potential of the ion source block and tuning the rest of the ion optics to get a beam current of 1–2 nA for the mass selected ion. The ions were allowed to pass through an ion deflector, an octupole ion guide (q2), and through a set of einzel lenses. The ions collide with the surface at an angle of

45° with reference to the surface normal during the ion scattering experiment. The secondary ions generated by the ion collision were collected by a set of einzel lenses and analyzed by a quadrupole mass analyzer (Q3).

Figure 2(a) shows the results of SimIon simulation of a scattering experiment where 1 eV Ar^+ (m/z 40) was allowed to collide on a target. The target was grounded. The overall energy spread of the source ions in the SimIon simulation was 0.0238 eV. This energy is a summation of potential differences at the positions where the ions were created and addition of the allowed kinetic energy distribution which is 0.01 eV. The remaining amount was due to the potential differences at the different positions where ions were born. The computations indicate satisfactory results of ultralow

energy ion scattering onto the target with good ion transmission. In this simulation, the repeller was set at 2 V, ion region was set at 1 V, the ion energy at the target was found to be 1.45 eV. Overall transmission loss was found to be 52% at 1 eV and 56% for 3 eV. Ion spatial spread increased from 1 mm at the source to ~ 3 mm at the surface. The spread can be reduced, however, by tighter focusing, especially at a slightly higher ion energy of 3 eV where the spread is found to be ~ 2 mm. The optimized instrumental parameters derived from the simulations were used to arrive at the instrumental parameters. Figure 2(b) shows a schematic of the instrument with detailed description of the components. The instrument consists of three chambers (as mentioned above) where there are seven sections, namely, ionizer, Q1, ion bender, q2, scattering chamber, Q3, and TPD probe. Ionizer is composed of an ion volume, a tungsten filament, a repeller, and one electromagnetic lens (L1). From ionizer to Q1, there is gate valve, which also acts as a lens. This was especially chosen to reduce the length of ion trajectory while having a reduced gas load in the scattering chamber from the ion source. After the gate valve lens, ions are mass selected using the Q1 quadrupole assembly. Ions from the source are passed through Q1 entrance lens (Q1 ENT) and Q1 pre/post filter before entering the Q1 mass analyzer. Mass analyzed ions are then channeled through another set of lenses, Q1 pre/post and Q1 exit lens. After these lenses, ions are filtered through ion bender where neutrals, if any, are rejected. As ions come out from the ion bender, those enter the octupole ion guide (q2). The q2 is having q2 entrance lens (q2 ENT), octupole, and q2 exit lens (q2 EXIT). After that there is a set of einzel lenses which focus ions onto the target. During ion scattering experiment, when the target is placed 45° with respect to the surface normal, scattered ions are guided to the analyzer quadrupole Q3 by another stack of einzel lenses. These ions are passed through Q3 which consists of Q3 entrance lens (Q3 ENT), quadrupole, and Q3 exit lens (Q3 EXIT). Finally the ions are detected using a conversion dynode (CD) and a channel electron multiplier. During the TPD measurement, the target is rotated to 225° from its ion scattering position. In the TPD probe, there is an ionizer similar to the one described previously. Mass analyzer is similar to Q3. In order to reduce sampling of other regions of the sample holder during TPD, the mass spectrometer has a skimmer, placed in the front of the axial ionizer.

Molecular surfaces were prepared by depositing the corresponding vapors and gases which were in turn delivered very close to the substrate through 1/8 in. stainless steel tubes. The exposure was controlled by a leak valve. The gas-line helps to maintain uniform sample growth on the substrate. Delivery of molecules near the substrate ensured that the vapors were not deposited in unwanted areas. The deposition flux of the vapors was adjusted to ~ 0.1 ML/s. The thickness of the overlayers was estimated assuming that 1.33×10^{-6} mbar s = 1 ML. 1 ML ice layers have been estimated to be $\sim 1.1 \times 10^{15}$ water molecules/cm².³⁷ The partial pressure of the vapor inside the scattering chamber during deposition time was 1×10^{-7} mbar. The films were prepared on Ru substrate to make Ru@A (the symbolism implies the creation of layer A over Ru). The spectra presented here

were averaged for 75 scans and the data acquisition time was approximately 0.5 s per scan.

In addition to low energy ion scattering mass spectrometry and TPD probe, the chamber is fitted with RAIRS set-up. The RAIRS experiments were performed using a VERTEX 70 FT-IR spectrometer of Bruker. The IR beam was taken out from the spectrometer to an off-axis paraboloidal gold-coated mirror (focal length 250 mm) which focused the beam at $80^\circ \pm 7^\circ$ incident angle onto the Ru single crystal mounted on the cryostat. The reflected beam from the surface was collected by another gold-coated ellipsoidal mirror mounted on an adjustable base plate and ultimately focused onto the detector (see Fig. 1, item 10). The entire IR beam path was purged with dry nitrogen gas. A liquid N₂ cooled broadband mercury-cadmium-telluride (MCT) detector (specific detectivity $D^* \sim 5 \times 10^9$ cm Hz^{1/2}/W) was used for the range of 12 000–420 cm⁻¹. The negative absorption observed around 2080 cm⁻¹ appeared to be due to background deposition of CO on the clean surface. The total IR path length from the spectrometer exit to the surface is 32.8 cm and the detector is 24.7 cm away from the sample.

III. RESULTS

In order to measure the distribution of ion kinetic energy (K.E.) of the input beam, stopping potential measurements¹⁸ were performed at Q1. In this measurement, Q1 was kept in the RF (radio frequency) only mode and it transmits all ions formed in the source and Q3 was set to transmit the desired mass. Thereafter, a range of DC voltages are applied across the quadrupoles in order to stop the desired ions. When the ions are stopped at Q1, for example, intensity of the ions detected falls to zero. Figure 3 shows the results of stopping potential measurements of 1, 2, and 3 eV Ar⁺ ions. It is evident from the figure that for 1 eV ion, the energy spread is 49% which reduces substantially (5%) in the case of 3 eV ions. With further increase in the input ion kinetic energy up to 8 eV, the spread decreases to 2% (data not shown). It is important to note that this kind of ion energy spread is the best that has been achieved so far in such instrumentation.⁶ Increased spread at extremely low energy (1 eV) has been noted before.^{18,20} Stopping potential measurement in q2 using Ar⁺ (Q1 was set to select the desired ion and Q3 was kept in RF-only mode) showed the same energy spread like Q1 (Fig. 3(a)). After the collision on the Ru target, the stopping potential experiment performed in Q3 indicates a further increase in spread which is 0.52 eV (Fig. 3(b)). This shows the excellent performance of the instrument especially at ultra-low energy range.

After the initial characterization measurements, ion scattering experiment was performed with C₆D₆⁺ (m/z 84) on Ru(0001) at 10 K. The kinetic energy of the ions was 1–6 eV. The results of the experiments are shown in Fig. 4(a). The small shoulder peak next to C₆D₆⁺ is attributed to C₆D₅⁺. Figure 4(b) shows the result of chemical sputtering conducted on 100 ML D₂O grown on Ru(0001) at 10 K. The projectile was 50 eV Ar⁺. Signal at m/z 22 indicates D₃O⁺, result of chemical sputtering of D₂O, the peak m/z 42 is due to D₅O₂⁺.

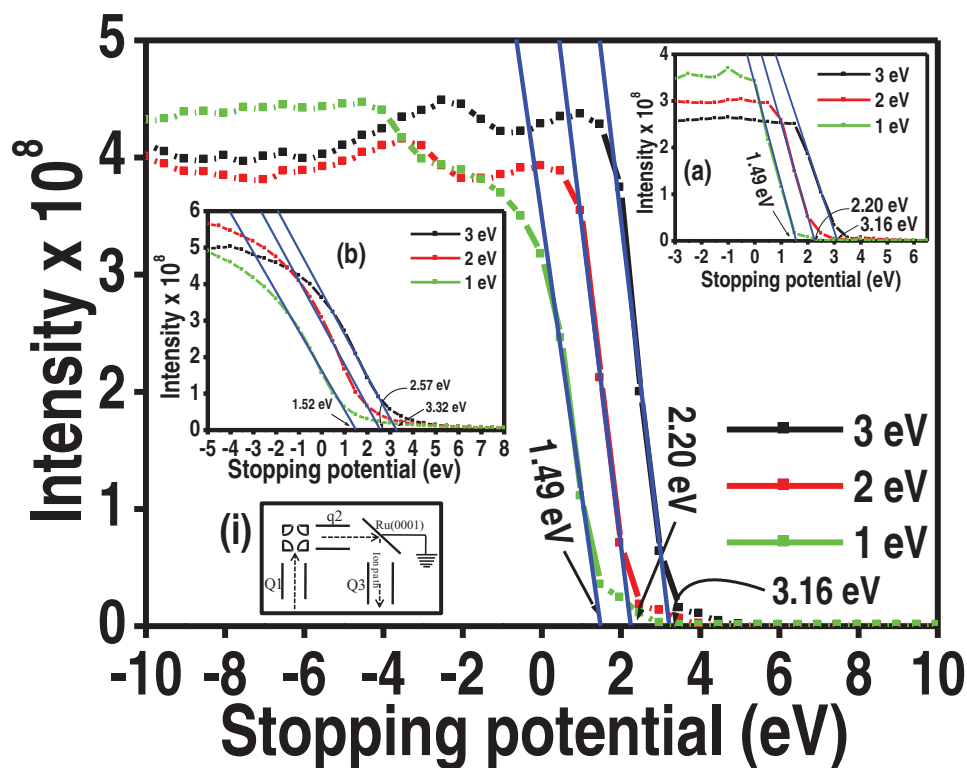


FIG. 3. Plot of Ar^+ stopping potential data at quadrupole 1 (Q1). Data corresponding to octupole 2 (q2) and quadrupole 3 (Q3) are in (a) and (b). The experimental scheme is shown in inset.

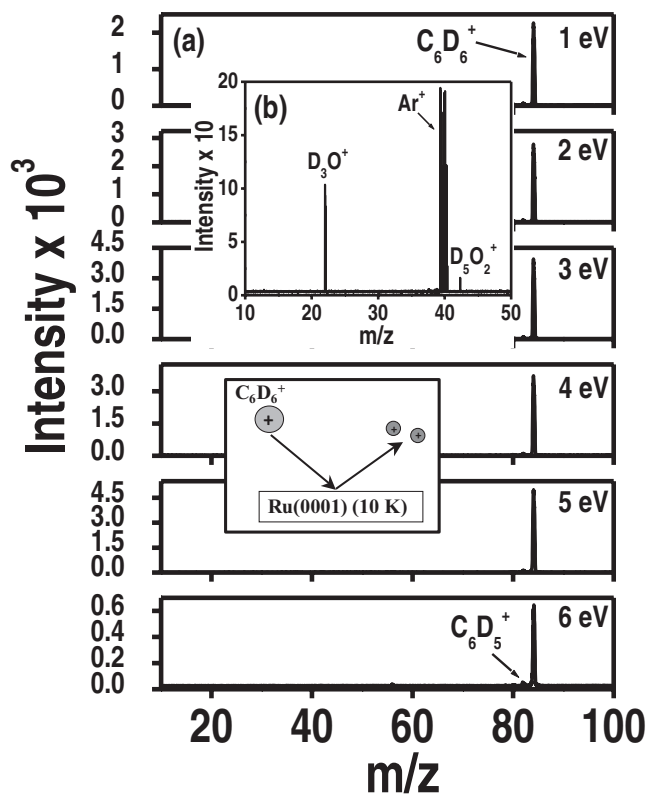


FIG. 4. (a) Results of 1–6 eV C_6D_6^+ scattering on Ru(0001) at 10 K. (b) Chemical sputtering spectrum due to 50 eV Ar^+ on amorphous ice at 100 K. Bottom inset shows a schematic of the ultralarge energy ion scattering experiment. The ejection of D_3O^+ is due to the proton-transfer reaction upon collision of Ar^+ ions ($2\text{D}_2\text{O} \rightarrow \text{D}_3\text{O}^+ + \text{OD}^-$).

The ions D_3O^+ and D_5O_2^+ are the characteristic features of D_2O ice. Note that no other ions such as hydrocarbons or H_3O^+ were seen which clearly demonstrate the cleanliness of vacuum, quality of the molecular film, and well-defined ion trajectory. In the absence of all these, the ion scattering spectrum could have shown several other features characteristic of impurities. These spectra indicate the successful performance of the instrument at the entire energy region for which the instrument was designed for.

Having established the instrument performance in the low to high energy window, we carried out TPD measurements. In this process, Argon was chosen as the atomic solid of choice. First the target was cooled to 10 K, which is well below the desorption temperature of Ar. After that, Ar gas was deposited through a leak valve in the scattering chamber for a certain period of time to develop the desired number of monolayers. Thereafter, the substrate was resistively heated at a constant rate (here 5 K/min). The resultant mass spectra were collected, where the surface was at the TPD position. Figure 5, inset (ii, bottom) shows one of the measured TPD spectra for 5 ML thickness of Ar. The ion intensity monitored in this case is m/z 40 due to Ar^+ . Next, a thickness dependent TPD experiment was performed where 0.5, 1, 2, 3, 5 ML of Ar was deposited and heated at the same rate as mentioned previously. From the resultant spectra, areas under the curve are plotted and presented in Fig. 5. Near linearity of the plot indicates successful performance of the TPD experiment at very low coverage and at very low temperature. Inset (ii) shows the TPD spectrum of 5 ML Ar. Curve fitting was done to find the multilayer and monolayer contributions in the TPD spectrum.

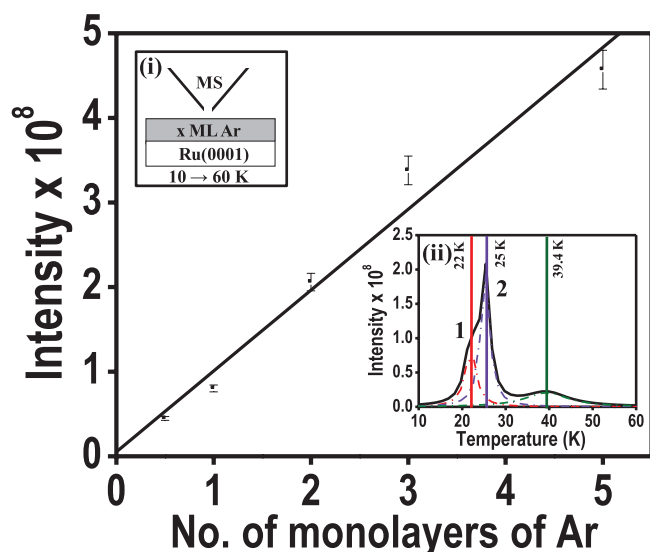


FIG. 5. Increase in intensity with respect to number of monolayers of Ar; 0.5, 1, 2, 3, 5 ML during the TPD experiment. Intensity refers to that of the m/z 40 peak. Inset (i) shows a schematic representation of the TPD experiment (MS stands for mass spectrometer). Inset (ii) shows the TPD spectrum of 5 ML Ar.

The residual Ar intensity beyond 30 K (maxima 39.4 K) is attributed to Ar desorption from regions other than the Ru crystal. This area is excluded in the total area measurement in the linear fit. The desorption spectrum is characterized by two peaks, the low temperature peak (marked as 1, maximum at 22 K) due to the multilayer and the high temperature peak (marked as 2, maximum at 25 K) due to the monolayer. Intensities of these two are used in the thickness evaluation.

Subsequently, reflection absorption infrared spectroscopy (RAIRS) was performed on 50 ML CCl_4 layer deposited on Ru at 100 K. Figure 6 shows the observed spectra. It is an average of 512 acquisitions with 4 cm^{-1} resolution. The spectrum shows the standard C–Cl stretching vibrations (ν_3) at 794 cm^{-1} and ν_1 (symmetric stretching) + ν_4 (degenerate deformation) modes of CCl_4 appear at

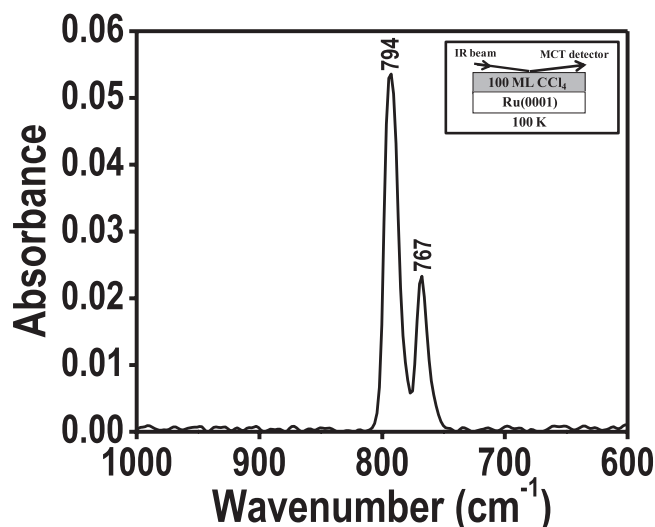


FIG. 6. RAIR spectrum of 100 ML CCl_4 deposited on Ru(0001) at 100 K.

767 cm^{-1} , respectively.^{38,39} This spectrum indicates excellent performance of the RAIRS set-up.

IV. CONCLUSION

The instrument developed shows excellent performance during ion scattering experiments in the ultralow energy range. Its capability to achieve low temperatures ($\sim 10 \text{ K}$) will help to study molecular and atomic solids of almost any gas (except hydrogen and helium). Simultaneous measurement of ion scattering, RAIRS, and TPD is expected to unravel various unexplored areas of molecular materials. A combination of all these data together can reveal the structure, reactivity, kinetics, and thermodynamics of surface processes. In conjunction with additional facilities such as low energy alkali ion sputtering, thermal evaporation along with surface activation by UV exposure, catalysis at molecular solids (photo and chemical) can be explored.

ACKNOWLEDGMENTS

T.P. acknowledges the Science and Engineering Research Board (SERB), Department of Science and Technology (DST), Government of India for funding. He also thanks the DST for continued support. S.B. and R.G.B. acknowledge Council of Scientific and Industrial Research (CSIR), Government of India for research fellowships. R.R.J.M. thanks the University Grant Commission (UGC) for his research fellowship.

- ¹R. G. Cooks, T. Ast, T. Pradeep, and V. Wysocki, *Acc. Chem. Res.* **27**, 316 (1994).
- ²S. A. Miller, H. Luo, S. J. Pachuta, and R. G. Cooks, *Science* **275**, 1447 (1997).
- ³J. Laskin, P. Wang, and O. Hadjar, *Phys. Chem. Chem. Phys.* **10**, 1079 (2008).
- ⁴S. Bag, R. G. Bhuin, G. Natarajan, and T. Pradeep, *Annu. Rev. Anal. Chem.* **6**, 97 (2013).
- ⁵G. E. Johnson, Q. Hu, and J. Laskin, *Annu. Rev. Anal. Chem.* **4**, 83 (2011).
- ⁶J. Cyriac, T. Pradeep, H. Kang, R. Souda, and R. G. Cooks, *Chem. Rev.* **112**, 5356 (2012).
- ⁷S. Nagaoka, T. Matsumoto, E. Okada, M. Mitsui, and A. Nakajima, *J. Phys. Chem. B* **110**, 16008 (2006).
- ⁸S. Nagaoka, K. Ikemoto, K. Horiuchi, and A. Nakajima, *J. Am. Chem. Soc.* **133**, 18719 (2011).
- ⁹S. Nagaoka, T. Matsumoto, K. Ikemoto, M. Mitsui, and A. Nakajima, *J. Am. Chem. Soc.* **129**, 1528 (2007).
- ¹⁰S. Nagaoka, K. Ikemoto, T. Matsumoto, M. Mitsui, and A. Nakajima, *J. Phys. Chem. C* **112**, 15824 (2008).
- ¹¹H. L. de Clercq, A. D. Sen, A. K. Shukla, and J. H. Futrell, *Int. J. Mass Spectrom.* **212**, 491 (2001).
- ¹²A. K. Shukla and J. H. Futrell, *Rev. Sci. Instrum.* **74**, 168 (2003).
- ¹³R. G. Cooks, T. Ast, and M. A. Mabud, *Int. J. Mass Spectrom. Ion Process.* **100**, 209 (1990).
- ¹⁴H. Kang, *Acc. Chem. Res.* **38**, 893 (2005).
- ¹⁵E.-S. Moon, J. Yoon, and H. Kang, *J. Chem. Phys.* **133**, 044709 (2010).
- ¹⁶R. J. W. E. Lahaye and H. Kang, *Chem. Phys. Chem.* **5**, 697 (2004).
- ¹⁷S. Bag, M. R. S. McCoustra, and T. Pradeep, *J. Phys. Chem. C* **115**, 13813 (2011).
- ¹⁸S. Bag, R. G. Bhuin, and T. Pradeep, *J. Phys. Chem. C* **117**, 12146 (2013).
- ¹⁹J. Cyriac and T. Pradeep, *J. Phys. Chem. C* **112**, 1604 (2008).
- ²⁰J. Cyriac and T. Pradeep, *J. Phys. Chem. C* **112**, 5129 (2008).
- ²¹B. M. Jones and R. I. Kaiser, *J. Phys. Chem. Lett.* **4**, 1965 (2013).
- ²²C. J. Bennett, S. J. Brotton, B. M. Jones, A. K. Misra, S. K. Sharma, and R. I. Kaiser, *Anal. Chem.* **85**, 5659 (2013).
- ²³S. J. Brotton and R. I. Kaiser, *Rev. Sci. Instrum.* **84**, 055114 (2013).

- ²⁴S. J. Brotton and R. I. Kaiser, *J. Phys. Chem. Lett.* **4**, 669 (2013).
- ²⁵Y. Guo, X. Gu, E. Kawamura, and R. I. Kaiser, *Rev. Sci. Instrum.* **77**, 034701 (2006).
- ²⁶W. Choi, C. Kim, and H. Kang, *Surf. Sci.* **281**, 323 (1993).
- ²⁷W. Y. Choi, T. H. Kang, and H. Kang, *Bull. Korean Chem. Soc.* **11**, 290 (1990).
- ²⁸S. J. Han, C. W. Lee, C. H. Hwang, K. H. Lee, M. C. Yang, and H. Kang, *Bull. Korean Chem. Soc.* **22**, 883 (2001).
- ²⁹R. Souda, H. Kawanowa, M. Kondo, and Y. Gotoh, *J. Chem. Phys.* **119**, 6194 (2003).
- ³⁰J. Cyriac, M. Wleklinski, G. Li, L. Gao, and R. G. Cooks, *Analyst* **137**, 1363 (2012).
- ³¹W.-P. Peng, M. P. Goodwin, Z. Nie, M. Volny, Z. Ouyang, and R. G. Cooks, *Anal. Chem.* **80**, 6640 (2008).
- ³²Z. Nie, G. Li, M. P. Goodwin, L. Gao, J. Cyriac, and R. G. Cooks, *J. Am. Soc. Mass Spectrom.* **20**, 949 (2009).
- ³³V. Grill, J. Shen, C. Evans, and R. G. Cooks, *Rev. Sci. Instrum.* **72**, 3149 (2001).
- ³⁴J. Cyriac and T. Pradeep, *J. Phys. Chem. C* **111**, 8557 (2007).
- ³⁵S. Usharani, J. Srividhya, M. S. Gopinathan, and T. Pradeep, *Phys. Rev. Lett.* **93**, 048304 (2004).
- ³⁶J. Cyriac and T. Pradeep, *Chem. Phys. Lett.* **402**, 116 (2005).
- ³⁷E.-S. Moon, H. Kang, Y. Oba, N. Watanabe, and A. Kouchi, *Astrophys. J.* **713**, 906 (2010).
- ³⁸A. J. Wagner, C. Vecitis, and D. H. Fairbrother, *J. Phys. Chem. B* **106**, 4432 (2002).
- ³⁹D. R. Lide, *CRC Handbook of Chemistry and Physics*, 82nd ed. (CRC Press, 2001).